

## A ‘sidewinding’ locomotion gait for hyper-redundant robots

J. W. BURDICK, J. RADFORD and G. S. CHIRIKJIAN\*

*Department of Mechanical Engineering, Mail Code 104-44, California Institute of Technology,  
Pasadena, CA 91125, USA*

*\*Department of Mechanical Engineering, 124 Latrobe Hall, Johns Hopkins University, Baltimore,  
MD 21218, USA*

Received for AR 5 December 1993

**Abstract**—This paper considers a novel form of hyper-redundant mobile robot locomotion which is analogous to the ‘sidewinding’ locomotion gait employed by several species of snake. It is shown that this gait can be generated by a repetitive traveling wave of mechanism deformation. This paper considers primarily the kinematics of the sidewinding gait. The kinematic analysis is based on a continuous ‘backbone curve’ model which captures the robot’s important macroscopic features. Using this continuous model, we first develop algorithms which enable travel in a uniform direction. We subsequently extend this basic gait pattern to enable changes in the direction of travel.

### 1. INTRODUCTION

Hyper-redundant robotic systems have a very large or infinite relative degree of kinematic redundancy. They are analogous to snakes, worms or elephant trunks. Many conceivable applications require the hyper-redundant robot to maneuver, via some form of locomotion, around its environment. This paper considers one possible way to implement hyper-redundant robot locomotion.

**DEFINITION.** Hyper-redundant robot ‘locomotion’ is the process by which net displacement of a hyper-redundant mobile robot arises from internally induced bending and twisting of the mechanism. Actuatable wheels, tracks or legs are not necessary.

**DEFINITION.** A hyper-redundant robot gait is a repetitive sequence of mechanism deformations which enables the net locomotive displacement.

For a given mechanism, different gaits will have correspondingly different speed, robustness and maneuverability characteristics. A gait which is well suited to one type of terrain or task may be ill suited to another situation. For maximum adaptability, a hyper-redundant robot should be capable of switching between several different gait types.

In [1, 2] we developed two classes of hyper-redundant robot gaits which were based on standing or traveling waves of mechanism distortion. These gaits, which enable locomotion along a curvilinear path, are idealizations of gaits used by inchworms, earthworms and slugs. Some of the gaits used by snakes, such as the creeping gaits employed in predation [3], can also be modeled using the methods of [2]. These locomotion schemes have been implemented and their viability demonstrated in an actual 30 d.o.f. hyper-redundant robot mechanism [2, 4].

However, other forms of locomotion used by creatures with hyper-redundant morphologies may not fit into either of these previously analyzed gait classes. In particular, snakes also employ sidewinding, concertina and undulating gaits [3]. This paper develops and analyzes a novel locomotion scheme which is qualitatively identical to the sidewinding locomotion of desert snakes.

We study this problem for two reasons. First, sidewinding motion is one of the most complicated forms of locomotion seen in nature. A better insight into the mechanics of this gait can lead to a broader understanding of robotic locomotion. Second, in previous work the authors have undertaken a broadly-based program to overcome some of the obstacles which currently prevent widespread and practical deployment of hyper-redundant, or snake-like, robotic systems. The ability to locomote in a variety of context- and task-dependent ways is vitally important to practical hyper-redundant robotic applications. The sidewinding motion analyzed in this paper is yet another means of hyper-redundant robot mobility that can be added to our previously developed repertoire. Empirical evidence indicates that the sidewinding gait can generate greater acceleration than other gaits. Thus, sidewinding would be most useful for implementing fast gross displacement, while the algorithms in [2] would be most useful for precise locomotory movements.

To our knowledge, there have been no previous analytical studies in the robotics literature concerning sidewinding gaits. However, many researchers have investigated hyper-redundant, or ‘snake-like’, robotic systems. For a history of the mechanical design and kinematics research in this area, see [5, 6]. Here we focus on prior work in hyper-redundant robot locomotion. To our knowledge, the ‘active cord’ mechanism of Hirose and Umetani [7] was the first hyper-redundant robotic system to successfully demonstrate locomotion. Hirose [8] has also extensively investigated a gait which is analogous to the undulatory gait commonly employed by many snakes. Hirose and coworkers have developed and demonstrated numerous mobile hyper-redundant mechanisms and mechanical morphologies, see [8, 9] and references therein. While some of these hyper-redundant mobile robots are a hybrid between a snake-like vehicle and a wheeled vehicle, we consider locomotion schemes which do not rely on actuatable wheels, tracks or legs. A conceptual scheme for locomotion of a Variable Geometry Truss (VGT) robot is discussed in [10], though no explicit analysis or algorithms for locomotion are given. Others have developed ‘inch-worming’ devices for crawling through pipes [11].

While the robotics literature is devoid of previous studies on sidewinding gaits, a number of biologists have examined sidewinding [3, 12–16]. In general, these previous works were highly qualitative or empirical. Here we give the first quantitative description of sidewinding motion.

## 2. QUALITATIVE DESCRIPTION OF SIDEWINDING LOCOMOTION

Figure 1 schematically depicts a snake undergoing sidewinding locomotion. One notices two interesting facts while observing a sidewinding snake. First, the snake appears to be moving sideways. Second, if the snake is moving uniformly across a sandy surface, a set of parallel tracks, which are neither parallel nor perpendicular to the direction of motion, will be left in the sand after the snake passes. Let these tracks be called *ground contact tracks* (GCTs). For travel in a uniform direction, the GCTs will be parallel lines. However, Section 5 will show that these tracks may assume more complicated forms during turning maneuvers. The portions of the snake in contact with the ground will henceforth be termed the *ground contact segments* (GCSs). A GCS is at rest with respect to the ground, i.e. it does not slip on the terrain.

Net snake displacement, or locomotion, is produced by moving the snake to sequential GCTs. The sequence of displacements is periodic and proceeds as follows. The sidewinding cycle begins with the head of the snake lifting from the current GCT and moving toward the next GCT. The lifted portion is termed an *arch segment*. The body is peeled away from the most forward ground contact track until almost one-quarter of the snake's body is cantilevered. A point just behind the head touches the ground, establishing a point on the next GCT.

Successive body segments are 'laid' down along this newly established GCT, while segments are simultaneously 'peeled' away from the prior GCT. The length of a fully formed GCS remains constant because the 'peeling' and 'laying' are done at the same rate. In this way, a GCS effectively travels the length of a GCT, even though the GCSs are at rest with respect to the ground. Because each contact segment travels the length of the entire snake, each line left behind in the sand is approximately the length of the snake.

After a certain amount of the snake is in contact with the forward GCT, the process is repeated. For most snakes, the body straddles three GCTs, or two during transitory

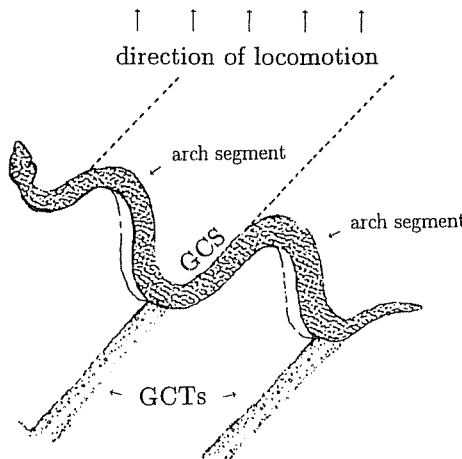


Figure 1. Schematic of a sidewinding snake.

phases. Thus, the steady state geometry of the sidewinding form is composed of multiple ground contact and arch segments. The net direction of snake travel is the sum of two components. The first is parallel to the GCT and arises from the motion of the ground contact segment along the track. The second component comes from the fact that the snake is continually reaching toward a new GCT.

One could imagine that sidewinding motion arises from a series of ‘waves’, where each wave is an arch segment that travels from the head of the snake to the tail. The GCSs are the interludes between the passing waves. In Section 4 we show that sidewinding can in fact be generated by a traveling wave of mechanism distortion. This traveling wave nature of the sidewinding gait is consistent with numerous experimental and analytical studies of the nervous systems of snakes and related animals (such as lampreys) which locomote via undulatory motion [17]. These studies show that the component of the nervous system which controls locomotion supports traveling waves of electrical activity. These rhythmic patterns of neural oscillation in turn drive the muscle contractions which generate undulatory locomotion.

Not all snake species employ sidewinding. Further, a sidewinding species may choose other gaits in a given situation. There are two plausible reasons why some snakes choose sidewinding. First, experimental evidence indicates that sidewinding can generate the greatest acceleration. This is not difficult to understand in light of the above discussion. The GCSs afford a large surface area of contact between the ground and the snake. Further, the friction between the snake and the ground is static, and not sliding, friction. Thus, sidewinding snakes can generate large reaction forces at the GCS. These forces can in turn generate rapid acceleration. Further, because these reaction forces are distributed over two or more GCSs, the sidewinding geometry is very stable. Second, desert dwelling snakes in particular may prefer sidewinding motion because it prevents overheating while traversing hot desert sands. Only small portions of the snake are in contact with the hot desert sand, while the remaining segments are repeatedly cooled when they are lifted in the air.

In the rest of this article, the important kinematic phenomena of the sidewinding gait are abstracted in terms of a ‘backbone curve’, which is reviewed in the next section.

### 3. KINEMATICS OF HYPER-REDUNDANT ROBOT BACKBONE CURVES

We assume that regardless of mechanical implementation, the important macroscopic features of a hyper-redundant robot can be captured by a *backbone curve* and associated set of reference frames which evolve along the curve. A backbone curve can be thought of as the curve which is a continuous approximation to the spine or centerline of the hyper-redundant mechanism [6, 18]. A backbone curve parametrization and set of reference frames are collectively referred to as the *backbone reference set*. In this paradigm, inverse kinematics and trajectory planning tasks are reduced to the determination of the proper time varying behavior of the backbone reference set. Depending upon the actual mechanical implementation of the robot, the associated backbone curve may be *non-extensible* (or fixed length) or *extensible* (variable

length). We review here the kinematics of non-extensible backbone curves. Extensible backbone curve kinematics, which are not needed in the sidewinding gait, can be found in [5, 6, 18].

### 3.1. A backbone reference set parametrization

The Cartesian position of points on a non-extensible backbone curve can be parametrized by:

$$\vec{x}(s, t) = \int_0^s \vec{u}(\sigma, t) d\sigma, \quad (1)$$

where  $s$  is the arclength parameter at time  $t$ , i.e.  $|\partial \vec{x} / \partial s| = 1$ . We often assume that distance is normalized so that  $s \in [0, 1]$ .  $\vec{x}(s, t)$  is a position vector from the base of the backbone curve to the point on the backbone curve denoted by curve parameter  $s$ . The base is defined as the point  $s = 0$ .  $\vec{u}(s, t)$  is the unit tangent vector to the curve at  $s$ . The parametrization of equation (1) has the following interpretation. The backbone curve is 'grown' from the base by propagating the curve forward along the backbone curve tangent vector, which is varying its direction according to  $\vec{u}(s, t)$ .

Any parametrization of the unit sphere can be used to parametrize  $\vec{u}(s, t)$  in (1). The explicit time dependence will often be suppressed for clarity of presentation, e.g.,  $\vec{u}(s, t)$  will often be written as  $\vec{u}(s)$ , etc. In this work, we select:

$$\vec{u}(\cdot) = [\sin K(\cdot) \cos T(\cdot), \cos K(\cdot) \cos T(\cdot), \sin T(\cdot)]^T, \quad (2)$$

where  $K(s)$  and  $T(s)$  are angles which determine the direction of  $\vec{u}(s)$  with respect to the reference frame attached to the backbone curve base ( $s = 0$ ) (see Fig. 2). By convention, the initial conditions  $K(0) = T(0) = 0$  are assumed.

Note that this alternate parametrization can be related to the classical Frenet–Serret method for parametrizing curves, as follows:

$$\begin{aligned} \kappa^2 &= (\dot{T})^2 + (\dot{K})^2 \cos^2 T, \\ \tau &= \dot{K} \sin T - \frac{(\dot{T} \ddot{K} - \ddot{T} \dot{K}) \cos T - (\dot{T})^2 \dot{K} \sin T}{\kappa^2} \end{aligned} \quad (3)$$

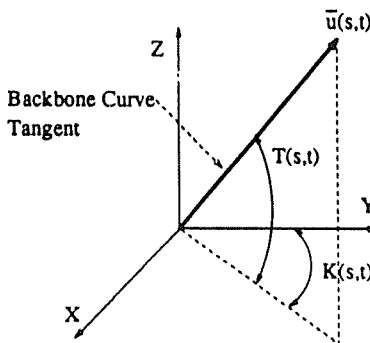


Figure 2. Definitions of  $K(s, t)$  and  $T(s, t)$ .

where  $\kappa$  and  $\tau$  are, respectively, the curvature and torsion of the backbone curve [19], and a dot represents differentiation with respect to  $s$ .

In summary, the backbone curve, which describes the important macroscopic shape of a hyper-redundant manipulator, is a function of a reduced set of intrinsic ‘shape functions’. For non-extensible spatially deforming backbone curves, two intrinsic functions uniquely define the backbone curve shape. Here we use  $K(s, t)$  and  $T(s, t)$ , although any spherical parametrization of  $\vec{u}(s, t)$  is acceptable. Alternatively, one could parametrize the backbone curve with the classical curvature and torsion functions:  $\kappa(s, t)$  and  $\tau(s, t)$ . The complete configuration of a non-extensible spatial hyper-redundant robot requires a third independent function, called the *roll distribution* [18], which measures how the manipulator twists about the backbone curve. We neglect this coordinate here, as the sidewinding gait is nominally independent of the roll distribution.

The backbone curve is an abstraction of a real hyper-redundant robot geometry. A continuous backbone curve shape, which is computed as the solution to a motion planning problem, can be directly used to determine the actuator displacements of hyper-redundant mechanisms with continuously deformable structures, such as those actuated by tendons or pneumatic/hydraulic structures. However, to apply this framework to discretely segmented hyper-redundant morphologies, a ‘fitting’ procedure is required. The goal of this fitting procedure is to determine the actuator displacements of the discrete morphology robot so that it exactly or closely follows the backbone curve model. We do not dwell on this aspect, as it is adequately treated in [6, 18]. The spatial Stewart platform fitting algorithm of [18] is used in ensuing examples.

#### 4. IDEALIZED SIDEWINDING LOCOMOTION: THE UNIFORM DIRECTION CASE

This section considers in detail how to construct a sidewinding gait for motion in a uniform direction. The following section will extend these results to enable changes in motion direction. We assume the hyper-redundant robot is locomoting on flat ground.

In light of the discussion in Section 2, the sidewinding gait can be idealized as a form of traveling wave locomotion in which the arch segment shape is a ‘wave’ that propagates from the head to the tail. The goal of this section is to synthesize the backbone curve shape functions which implement the sidewinding gait. For simplicity, we shall choose to construct the shape functions in the  $K(s, t)$ – $T(s, t)$  shape function coordinates.

The following notation and assumptions are used in the sequel:

- (1) The backbone curve is non-extensible, with arclength parameter  $s$ .  $s = 0$  is the ‘head’ of the backbone curve.
- (2) At a given instant of time, let the snake be in contact with the ground via  $N$  ground contact segments. Index these segments by  $j$ , with  $j = 1$  indexing the segment closest to the head. Note that some of these segments may be not be fully formed at any instant.
- (3) Let the arc-length of the backbone curve segment contained in the  $j$ th fully formed GCS be denoted by  $L_{gj}$ . Similarly, let  $L_{aj}$  denote the arc-length of the

$j$ th fully formed arch segment. Typically, these lengths are uniform for all fully formed ground contact and arch segments:  $L_{a_j} = L_a$  and  $L_{g_j} = L_g$ . However, the ensuing analysis does not make this assumption. Note that  $L_{g_j}$  may be zero, implying that the GCS is merely a point.

- (4) Let  $s_{j,1}(t)$  and  $s_{j,2}(t)$  denote the most forward and rearward points of the  $j$ th GCS (see Fig. 3). Similarly, let  $s_{j,3}(t)$  denote the most rearward point of the  $j$ th arch segment.  $s_{j,1}(t)$ ,  $s_{j,2}(t)$  and  $s_{j,3}(t)$  move along the backbone curve with wave speed  $\omega$ :  $ds_{j,1}(t)/dt = ds_{j,2}(t)/dt = ds_{j,3}(t)/dt = \omega$ . In this idealized flat ground case where the snake is moving in a uniform direction, we assume that  $s_{j,2}(t) = s_{j,1}(t) + L_{g_j}$  and  $s_{j,3}(t) = s_{j,2}(t) + L_{a_j}$ .

The problem of determining the global backbone curve shapes which implement sidewinding motion can be decomposed into the following steps:

- (1) Find the static arch and ground contact segment shapes that satisfy necessary geometric constraints.
- (2) Ensure that the arch and ground contact segment shapes blend smoothly at their intersection.
- (3) Convert the resulting shape to a traveling wave form. That is, for shape function  $\mathcal{S}(s, t)$ :  $\mathcal{S}(s, t) \rightarrow \mathcal{S}(s - \alpha_t(t), t)$ , where  $\alpha_t(t)$  takes the form:

$$\alpha_t(t) = \omega \left[ t - I \left( t, \frac{L_a + 1}{\omega} \right) \right] - L_a, \quad (4)$$

where  $I(t, t_p) = t_p \lfloor (t/t_p) \rfloor$  (see [1, 2] for definitions and notation).

The choice of  $\alpha_t(t)$  in equation (4) induces a constant velocity wave of mechanism deformation, whose shape is defined by the arch segment geometry, to travel the length of the backbone curve with speed  $\omega$ . The wave repeats at period  $(L_a + 1)/\omega$ , causing continuous periodic motion. One wave is required for each active arch segment.

The total backbone shape can then be constructed as the piecewise sum of shape functions which separately control the shapes of the arch segments and the ground contact segments:

$$K(s, t) = \sum_{j=1}^N K_{g_j}(s - \alpha_t(t)) W(s - \alpha_t(t), s_{j,1}, s_{j,2}) + K_{a_j}(s - \alpha_t(t)) W(s - \alpha_t(t), s_{j,2}, s_{j,3}), \quad (5)$$

$$T(s, t) = \sum_{j=1}^N T_{g_j}(s - \alpha_t(t)) W(s - \alpha_t(t), s_{j,1}, s_{j,2}) + T_{a_j}(s - \alpha_t(t)) W(s - \alpha_t(t), s_{j,2}, s_{j,3}), \quad (6)$$

where  $W(\cdot)$  is a *window function*:

$$W(s, s_0, s_1) = \begin{cases} 1 & \text{for } s \in [s_0, s_1], \\ 0 & \text{otherwise.} \end{cases} \quad (7)$$

$K_{a_j}(s, t)$ ,  $T_{a_j}(s, t)$ ,  $K_{g_j}(s, t)$  and  $T_{g_j}(s, t)$  are, respectively, the shape functions for the  $j$ th arch and ground contact segments of the backbone curve.

The GCSs are straight lines for sidewinding motion over flat ground. Consequently,  $K_{g_j}(s, t)$  and  $T_{g_j}(s, t)$  assume the simple forms (for all  $j$ ):

$$K_g(s, t) = 0, \quad T_g(s, t) = 0. \quad (8)$$

The next subsection develops constraints for the class of functions which can be arch segment shape functions.

#### 4.1. The arch segment shape functions

In this section we focus on a single arch segment, as this is the simplest unit of the sidewinding gait geometry. Nearly all of the important attributes of the gait are determined by the arch segment.

Consider the  $j$ th arch segment. For convenience, we drop the subscript  $j$ , though it is implicit. Assign two local coordinate systems,  $F_2$  and  $F_3$ , at  $s_{j,2}$  and  $s_{j,3}$  (Fig. 3). Let the  $x$ -axes of these coordinate frames, respectively denoted  $\hat{x}_{j,2}$  and  $\hat{x}_{j,3}$ , be collinear with the GCTs. Equivalently, they are collinear with the backbone curve tangent at  $s_{j,2}$  and  $s_{j,3}$ . Let the respective  $z$ -axes, denoted by  $\hat{z}_{j,2}$  and  $\hat{z}_{j,3}$ , be normal to the plane of locomotion, while the  $y$ -axes are chosen to complete coordinate system using the right-hand-rule.

Let us introduce a normalized arc-length on the arch segment:  $\xi = (s - s_{j,2})/L_{a_j}$ , i.e.  $\xi \in [0, 1]$ . Points along the arch segment, as measured in  $F_2$  can be parametrized as:

$$\vec{p}(\xi) = \begin{pmatrix} p_1(\xi) \\ p_2(\xi) \\ p_3(\xi) \end{pmatrix} = L_{a_j} \int_0^\xi \vec{u}_a(\sigma) d\sigma, \quad (9)$$

where  $\vec{u}_a(s)$  is the tangent vector to the arch segment in the interval  $s \in [s_{j,2}, s_{j,3}]$ . Further, we assume that the parametrization equation (2) is in effect:

$$\vec{u}_a(\xi) = [\cos K_a(\xi) \cos T_a(\xi), \sin K_a(\xi) \cos T_a(\xi), \sin T_a(\xi)]^T. \quad (10)$$

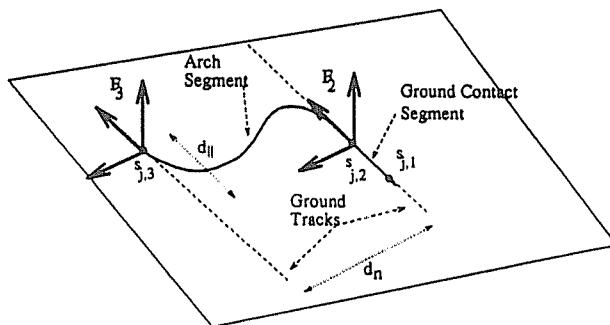


Figure 3. Identified points and frames of an arch segment.

In this local coordinate system, the arch segment must satisfy:

$$\begin{aligned}\vec{p}'(0) &= \hat{\mathbf{x}}_{j,2} = [1, 0, 0]^T = \text{tangent to ground contact track at } s_{j,2}, \\ \vec{p}(1) &= \vec{x}(s_{j,3}) - \vec{x}(s_{j,2}) = [d_{||}, d_n, 0]^T, \\ \vec{p}'(1) &= \hat{\mathbf{x}}_{j,3} = \text{tangent to ground contact track at } s_{j,3},\end{aligned}\quad (11)$$

where a prime indicates differentiation with respect to  $s$ .  $d_n$  is the distance between the parallel ground contact tracks, while  $d_{||}$  is the displacement of two ends of the arch segment along the ground contact line direction (Fig. 3).

For the case of parallel ground contact lines employed in uniform motion,  $\hat{\mathbf{x}}_{j,2} = \hat{\mathbf{x}}_{j,3} = [1, 0, 0]^T$ . Thus, to satisfy condition (11), we require that:

$$K_a(s_{j,2}) = K_a(s_{j,3}) = T_a(s_{j,2}) = T_a(s_{j,3}) = 0 \quad (12)$$

and:

$$\begin{aligned}L_a \int_0^1 \cos K_a(\xi) \cos T_a(\xi) d\xi &= d_{||}, \\ L_a \int_0^1 \sin K_a(\xi) \cos T_a(\xi) d\xi &= d_n, \\ L_a \int_0^1 \sin T_a(\xi) d\xi &= 0.\end{aligned}\quad (13)$$

We further require that:

$$\int_0^{\xi} \sin T(\xi) d\xi \geq 0 \quad \forall \xi \in [0, 1], \quad (14)$$

so that the arch segment does not touch the ground anywhere between its end points. Consequently, any functions  $K_a(s)$ ,  $T_a(s)$  which satisfy equations (12)–(14) are suitable candidates for the arch shape functions.

The problem of finding the shape of the arch section can also be posed as a hyper-redundant robot inverse kinematic problem. One can think of the arch segment as the backbone curve of a hyper-redundant manipulator whose base is located at  $\vec{x}(s_{j,2})$  and whose end-effector must reach  $\vec{x}(s_{j,3})$  with certain constraints on orientation. Two of the authors have previously developed schemes for solving this problem, using the intrinsic kinematic modeling scheme of Section 3 [6, 18, 20].

In one approach [20], the calculus of variations is used to find the shape functions which cause the manipulator (here, the arch segment) to satisfy necessary boundary conditions while also minimizing a user defined criteria, such as the total bending of the robot. This approach is physically appealing in this problem because it is likely that real snakes choose the shape of the arch segment to minimize some criteria, such as energy or total bending. However, this approach is computationally less attractive for the current application.

Alternatively, a ‘modal’ approach can be used to efficiently compute inverse kinematic solutions in a practically useful way [6, 18]. In this approach, the backbone curve shape functions are restricted to a modal form:

$$K_a(s, t) = \sum_{i=1}^{N_K} a_i(t) \phi_i(s); \quad T_a(s, t) = \sum_{i=N_K+1}^{N_K+N_T} a_i(t) \phi_i(s). \quad (15)$$

The  $\{\phi_i(s)\}$  are termed *mode functions*, while the  $\{a_i(t)\}$  are termed *modal participation factors*.  $N_K$  and  $N_T$  are, respectively, the number of modes distributed in the  $K$  and  $T$  shape functions. Their number must equal or exceed the number of geometric constraints on the respective shape functions. The  $\{\phi_i\}$  are specified by the user. For given  $\{\phi_i\}$ , the arch segment shape is determined by the  $\{a_i\}$ . The inverse kinematic problem reduces to the search for the proper  $\{a_i\}$  that satisfy the constraints. The next section shows by example how the mode shapes can be chosen to reflect the physical characteristics of the problem.

#### 4.2. An example

In general,  $F_3$  may be displaced relative to  $F_2$  with 6 d.o.f. However, for uniform motion on flat ground,  $F_3$  has only two relative degrees of freedom with respect to  $F_2$ , and thus only one mode need be distributed in each of the functions  $K_a$  and  $T_a$ . Assume  $K_a$  and  $T_a$  have the form:

$$K_a(s, t) = a_1(t) \phi_1(s), \quad T_a(s, t) = a_2(t) \phi_2(s). \quad (16)$$

To satisfy (12),  $\phi_1(s)$  and  $\phi_2(s)$  must assume zero value at the end points of the arch segment:  $\phi_1(s_{j,2}) = \phi_1(s_{j,3}) = \phi_2(s_{j,2}) = \phi_2(s_{j,3}) = 0$ . Additional physical insight into reasonable choices for  $\phi_1(s)$  and  $\phi_2(s)$  can be realized as follows.

Note that  $\sin T_a(s)$  encodes the vertical component of the tangent to the arch segment backbone curve. The vertical height of the arch segment should be increasing from zero at  $s_{j,2}$  to a point roughly in the middle of the arch segment, and then decreasing to zero afterwards. At the maximum height of the arch segment,  $T_a$  assumes zero value. While  $T_a(s)$  need not have any symmetry, for simplicity’s sake we assume  $\phi_2(s)$  is odd about the midpoint of the interval  $[s_{j,2}, s_{j,3}]$ . Thus, the maximum height of the arch segment occurs at  $\xi = 1/2$  and the arch height is uniformly increasing or decreasing on either side of this point.

$K_a$  nominally encodes the angle which the projection of  $\vec{u}(s)$  onto the locomotion plane makes with respect to the  $x_2$ -axis. Though  $K_a(s)$  need not have any symmetry, we again assume that  $K_a(s)$  is even about the midpoint of the arch segment. In this way, the arch segment has a nominally ‘S-shaped’ geometry.

Among the simplest shape functions which satisfy the above constraints and assumptions are the following piecewise continuous functions:

$$\phi_1(\xi) = \begin{cases} 2\pi\xi & \text{for } \xi \in [0, 1/2], \\ 2\pi(1 - \xi) & \text{for } \xi \in [1/2, 1], \end{cases} \quad (17)$$

$$\phi_2(\xi) = \begin{cases} 2\pi\xi & \text{for } \xi \in [0, 1/4], \\ \pi(1 - 2\xi) & \text{for } \xi \in [1/4, 3/4], \\ 2\pi(\xi - 1) & \text{for } \xi \in [3/4, 1]. \end{cases} \quad (18)$$

Substituting (17) and (18) into (2), a tedious calculation shows that at  $\xi = 1$ :

$$\begin{aligned} p_1(1) &= x_1(s_{j,3}) - x_1(s_{j,2}) = \frac{2 \cos\left(\frac{\pi a_1}{2}\right)}{\pi(a_1^2 - a_2^2)} \left[ a_1 \sin\left(\frac{\pi a_1}{2}\right) - a_2 \sin\left(\frac{\pi a_2}{2}\right) \right] L_a, \\ p_2(1) &= x_2(s_{j,3}) - x_2(s_{j,2}) = \frac{2 \sin\left(\frac{\pi a_1}{2}\right)}{\pi(a_1^2 - a_2^2)} \left[ a_1 \sin\left(\frac{\pi a_1}{2}\right) - a_2 \sin\left(\frac{\pi a_2}{2}\right) \right] L_a, \\ p_3(1) &= x_3(s_{j,3}) - x_3(s_{j,2}) = 0. \end{aligned} \quad (19)$$

Dividing the  $p_2$  component by the  $p_1$  component, it can be seen that:

$$a_1 = \frac{2}{\pi} \text{Atan} 2[(x_2(s_{j,3}) - x_2(s_{j,2})), (x_1(s_{j,3}) - x_1(s_{j,2}))] = \frac{2}{\pi} \text{Atan} 2[d_h, d_{\parallel}]. \quad (20)$$

Squaring and adding the first two components of (19),  $a_2$  can be found as the root to the following transcendental equation:

$$\beta a_2^2 - a_2 \sin\left(\frac{\pi a_2}{2}\right) = \beta a_1^2 - a_1 \sin\left(\frac{\pi a_1}{2}\right) \quad (21)$$

where  $a_1$  assumes the value computed using equation (20). This equation will have two roots in  $a_2$ , but due to symmetry properties of  $\phi_2(s)$ , both roots lead to the exact same shape. Figure 4 shows the actual geometry of an arch segment constructed using these shape functions for the case  $(p_1(1), p_2(1), p_3(1)) = (0.3, 0.6, 0.0)$ .

These simple mode functions are advantageous because they lead to nearly closed form solutions for the desired modal participation factor values. However, there are infinitely many other modal expansions of  $K_a$  and  $T_a$  which satisfy constraints (12)–(14) but do not have closed form solutions as above. The modal participation factors can be efficiently computed in these cases by using a method analogous to the 'resolved' rate trajectory planning approach. This method is derived as follows. The derivative of the forward kinematic map for a backbone curve segment restricted to modal form is:

$$\dot{\vec{p}} = \mathcal{T} \dot{\vec{a}}, \quad (22)$$

where  $\mathcal{T}$  is the *modal Jacobian* with elements:

$$T_{ik} = \frac{\partial p_i(1)}{\partial a_k}, \quad (23)$$

which is analogous to the traditional manipulator Jacobian matrix, only now modal participation factors are used instead of joint angles.

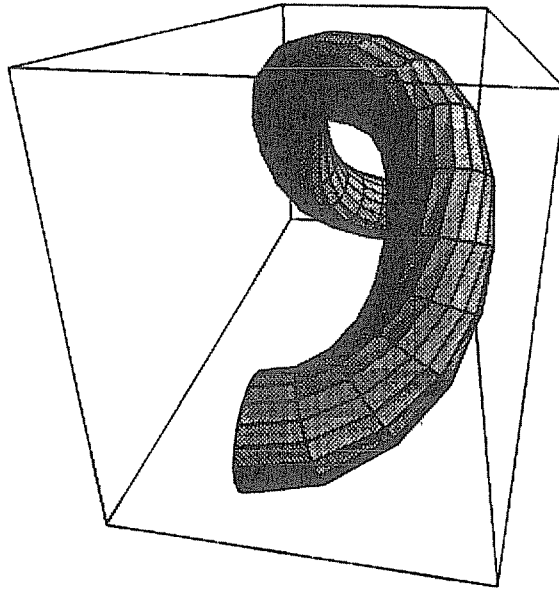


**Figure 4.** Example of arch segment geometry.

Equation (22) can be used in two ways. In the first method, if  $\vec{p}$  is time varying (as in Section 5) then (22) can be solved for  $\vec{a}$ . Assuming that a modal participation factor initial condition,  $\vec{a}(0)$ , is known, the inverse of (22) can be numerically integrated to find the time varying modal participation factors which cause the tip of the arch segment to track  $\vec{p}(t)$ .

Equation (22) can also be used in an iterative fashion to determine the correct  $\vec{a}$  for a given  $\vec{p}$ . For a given initial guess of modal participation factors,  $\tilde{\vec{a}}_0$ , the forward kinematic equations can be exactly or numerically solved to find  $\vec{p}(1)$ . This position will differ from the desired position because  $\tilde{\vec{a}}_0$  is an estimate. The following iteration will converge to the proper modal participation factors:

$$\tilde{\vec{a}}_k = \tilde{\vec{a}}_{k-1} + \alpha \mathcal{T}^{-1}(\tilde{\vec{a}}_{k-1})(\vec{p}_D - \vec{p}(\tilde{\vec{a}}_{k-1}, 1)). \quad (24)$$

$\vec{p}_D$  is the desired value of  $\vec{p}(1)$  (the touch down point of the arch segment as measured in  $F_2$ ), while  $\vec{p}(\tilde{\vec{a}}_k, 1)$  is the computed forward kinematics using the estimated modal participation values,  $\tilde{\vec{a}}_k$ . The index  $k$  indicates the iteration number.  $\alpha$  is a positive scalar which controls the convergence rate of the iteration. For small  $\alpha$  ( $\alpha \leq 1$ ), this iteration will converge to the proper set of modal participation factors which solves the modal inverse kinematic problem.

It is not always possible to compute the elements of the modal Jacobian in closed form. However, it is always possible to numerically compute the components using Liebnitz's rule. For example, if  $K_a$  and  $T_a$  have the forms of equation (16),  $\mathcal{T}$  is a

$2 \times 2$  matrix with components:

$$\begin{aligned}
 \mathcal{T}_{11} &= \frac{\partial p_1(1)}{\partial a_1} = L_{a_j} \int_0^1 \phi_1(\xi) \cos K_{\text{wave}}(\xi) \cos T_{\text{wave}}(\xi) d\xi, \\
 \mathcal{T}_{12} &= \frac{\partial p_1(1)}{\partial a_2} = -L_{a_j} \int_0^1 \phi_2(\xi) \sin K_{\text{wave}}(\xi) \sin T_{\text{wave}}(\xi) d\xi, \\
 \mathcal{T}_{21} &= \frac{\partial p_2(1)}{\partial a_1} = -L_{a_j} \int_0^1 \phi_1(\xi) \sin K_{\text{wave}}(\xi) \cos T_{\text{wave}}(\xi) d\xi, \\
 \mathcal{T}_{22} &= \frac{\partial p_2(1)}{\partial a_2} = -L_{a_j} \int_0^1 \phi_2(\xi) \cos K_{\text{wave}}(\xi) \sin T_{\text{wave}}(\xi) d\xi.
 \end{aligned} \tag{25}$$

Figure 5 shows three different arch segment backbone curve shapes side by side to indicate that a wide variety of mode shapes lead to very similar arch segment geometry. In each case, the participation factors were computed using the modal Jacobian approach. Thus we see that the choice of particular mode functions is often not highly critical to the success of this method.

Also note that a given choice of mode functions restricts the 'workspace' of the arch segment. That is, there is a limited range of location of the tip of the arch segment relative to the base of the arch segment for a given set of modes. This restriction in turn will limit the range of directions which the sidewinding robot can move.

In Fig. 6, the arch and ground contact segments are assembled into an entire snake. This mechanism will sidewind if the backbone curve segments are given the traveling wave form of (5) and (6). Figure 7 shows a sequence from a computer simulation of the sidewinding gait described in this section. The lines on the terrain surface show the evolution of the contact points as the sidewinding gait progresses.

If we define the 'average velocity',  $\langle v \rangle$ , of the sidewinding gait to be the net displacement that the head or tail of the backbone curve makes during one complete

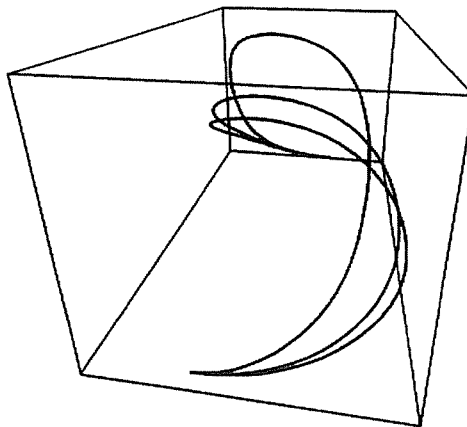


Figure 5. Three different arch segment shapes.

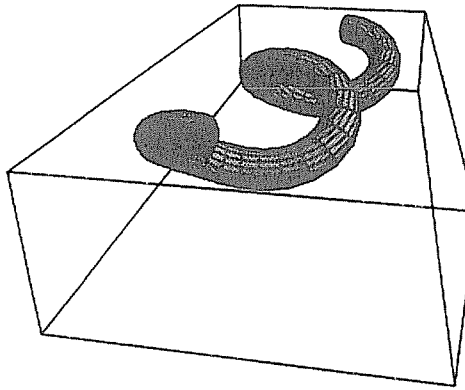


Figure 6. Idealized sidewinding shape.

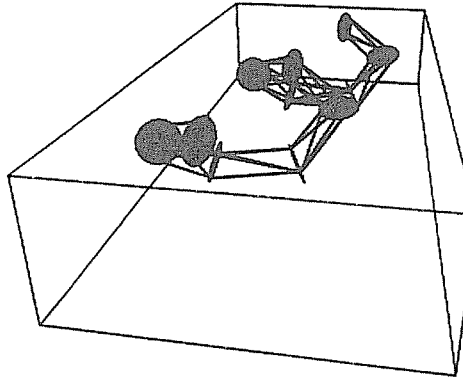


Figure 7. Stuart platform 'fitted' to backbone curve of Fig. 6.

wave cycle, then it can be shown that:

$$\langle v \rangle = \frac{N \sqrt{(L_a - d_{||})^2 + d_n^2}}{\omega}, \quad (26)$$

where we assume that  $L_{aj} = L_a$  for all  $j$ .

Note that the sidewinding gaits discussed in this section can also be implemented in robotic mechanisms which do not have a continuous morphology. Figure 8 shows a robot consisting of a concatenation of Stuart platforms. The fitting method of [18] is used to 'fit' this structure to the continuous backbone curve solutions. Figure 9 shows snapshots from a computer simulation in which this discrete morphology robot implements the sidewinding gait.

Note that in this section we assumed that the number of modes distributed in the arch segment mode functions equaled the number of geometric constraints on the arch segments (two). Additional modes can be added to generate more complex arch segment shapes. In this case, the modal Jacobian inverse in equation (24) is replaced by

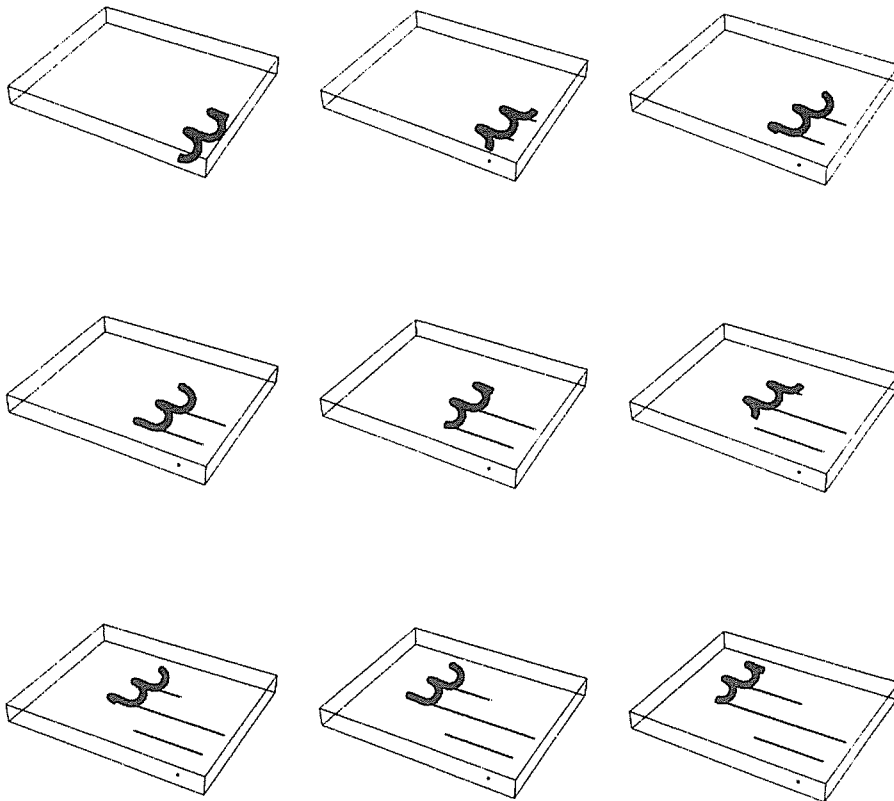


**Figure 8.** Snapshots of computer simulation of sidewinding kinematics.

its pseudo-inverse. Iteration of (24) will converge to the minimum norm modal participation factors which satisfy the geometric constraints. Modal Jacobian null space terms can be added to modify the internal geometry of the arch segment [6, 18].

## 5. TURNING AND CHANGES IN DIRECTION

This section considers ways in which a sidewinding hyper-redundant robot could change the direction of its nominal motion. Recall that the direction of travel is the sum of a component parallel to the GCT and one along a vector from the beginning of one arch segment to the beginning of the next. To turn, at least one of these components must change. Below we outline methods for modifying the direction of travel by modifying these components. Note that none of these methods involves sliding and thus the GCSs are always in contact with the environment via static friction.

### 5.1. Turning via head placement

A change in direction can be most simply effected by placing the head on the next GCT at a different relative position. This effect is demonstrated in Fig. 10 which

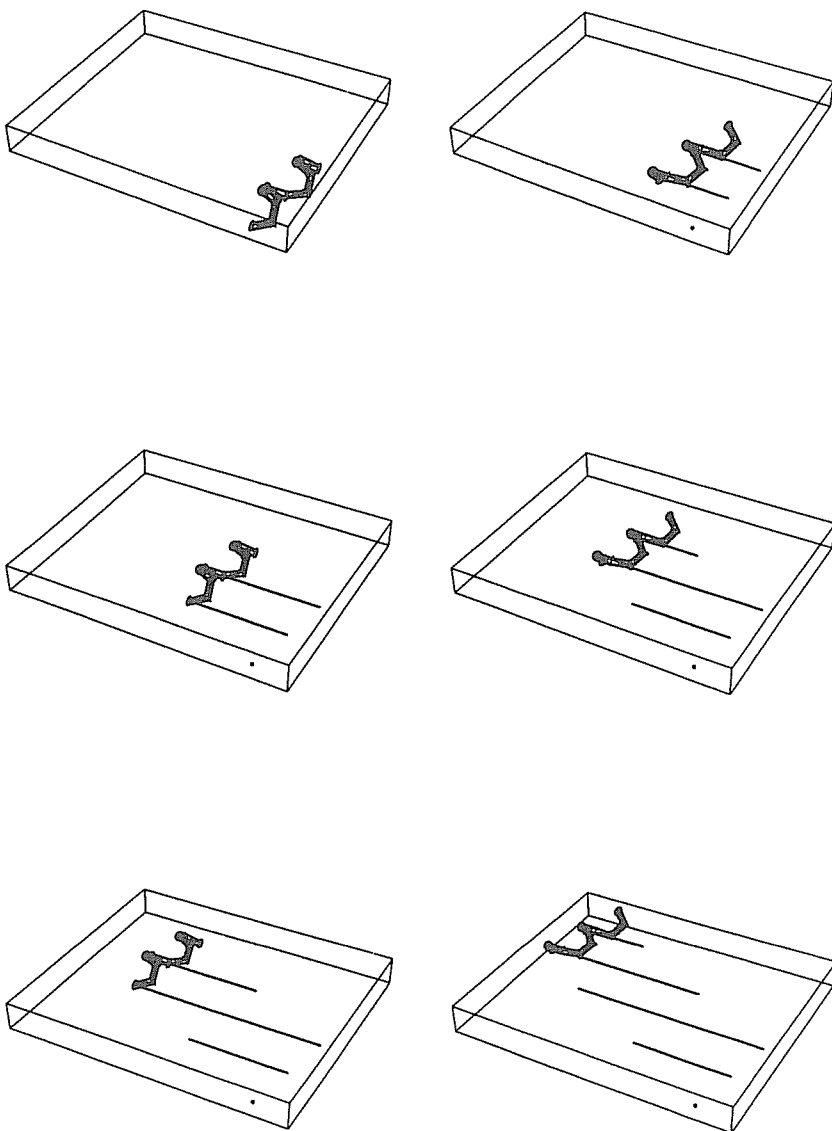


**Figure 9.** Discrete morphology robot implementing sidewinding motion.

depicts an overhead view of the backbone curve shape during a sequence in which the head abruptly changes its placement. Even though the GCTs remain parallel and the same distance apart, changing the arch displacement vector alters the net direction of travel. Note that it also alters the shape of the robot. This may be unacceptable in some cases, as the new shape required to move in a particular direction may lead to less efficient motion.

Temporary deviations from the nominal direction of motion can be implemented by a 'jog' (Fig. 11), in which the arch placement is altered only between one pair (or

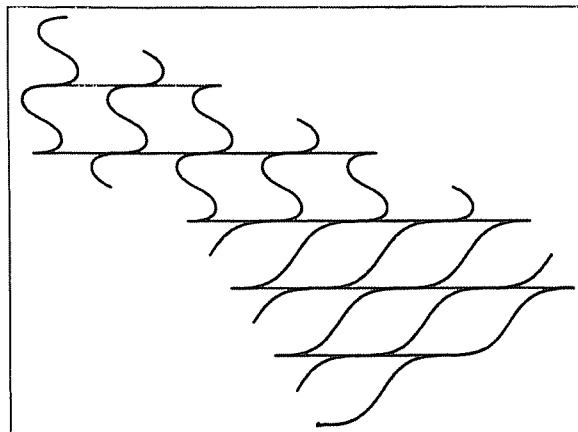


**Figure 10.** Turning by alternation of head placement.

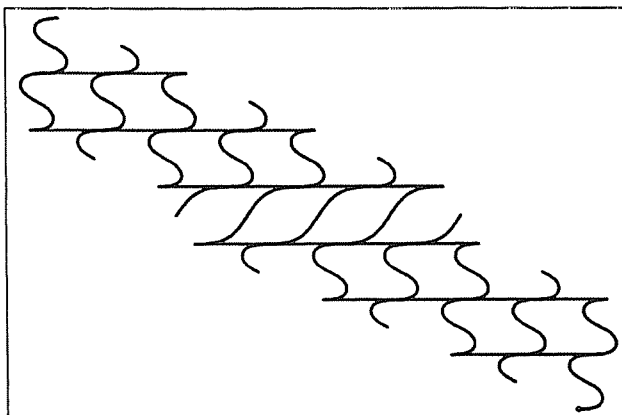


**Figure 11.** A 'jog' in arch placement.

a few pairs) of adjacent GCTs. The net direction of motion is the same before and after the jog. However, the path of the motion is displaced. This behavior is useful for detouring around obstacles. Since the robot has the same shape before and after the jog, this maneuver does not substantially slow the robot's progress.

### 5.2. Turning via skew GCTs

A change in direction can also be implemented by changing the angle between two successive GCTs from parallel to skew (Fig. 12). This is done during the arch segment forming phase. The head touches down on the next GCT so that the backbone curve tangent is at an angle to the previous track. All subsequent GCTs are parallel to this new skew track. This effects a change in motion in which the sidewinder shape is the same before and after the transition caused by the skew displacement.

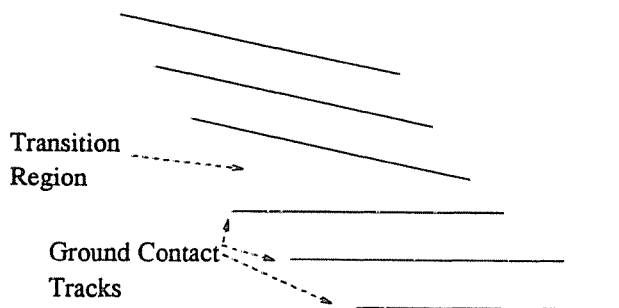


Figure 12. Turning via skew ground contact lines.

There is a limit of on the magnitude of the direction change that can be made using this method. The limiting process depends on the direction of the turn. If the skew angle is too large, then either the robot must intersect itself at some point during the motion or the distance between the skew GCTs may exceed the reach of the arch segment. Thus, this method is limited to shallow turns. Also note that in this form of turning, the shape of the arch segment must continuously change to accommodate the varying touch-down point. Thus, the arch segment can no longer be a traveling wave with a fixed wave shape. The modal Jacobian method discussed in Section 4 can be used to compute the values of the modal participation factors at each instant of time during the turning transition. However, at least three modes are required.

### 5.3. Turning by curvilinear GCTs

Turning can also be implemented by 'bending' the GCTs during the turning sequence. As in the skew method above, the ground contact lines are parallel before and after a turning transition region. However, in the turning transition region, the ground contact lines are curved to smoothly blend the two sets of parallel GCTs. During the

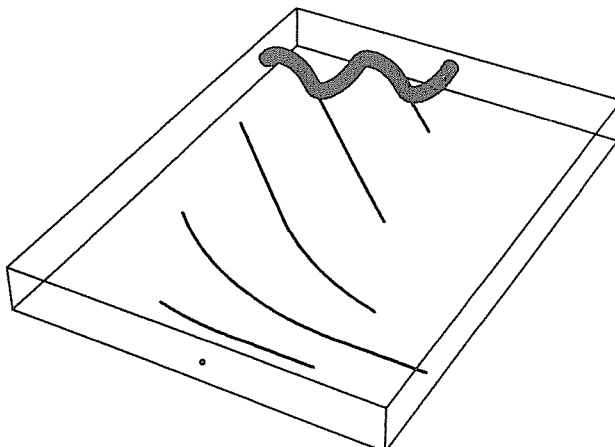
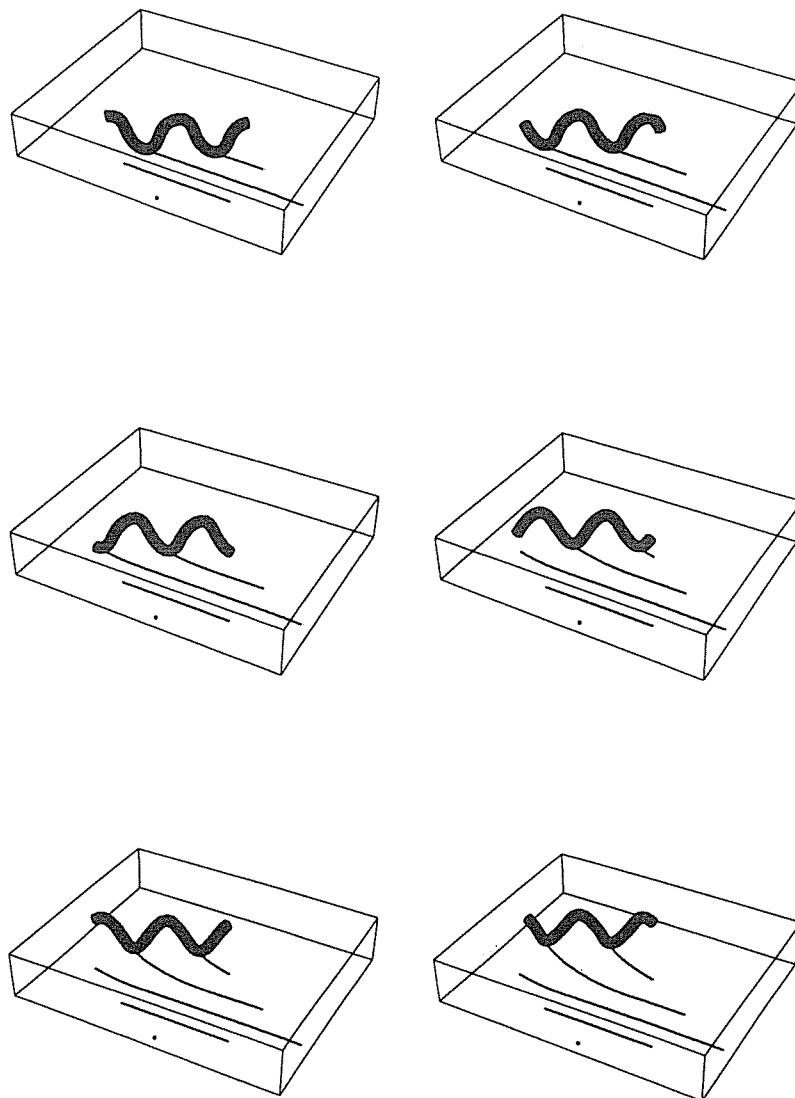


Figure 13. Turning via curved GCTs.



**Figure 14.** Snapshots of curvilinear turning simulation.

turning process, robot segments are laid down along the curved ground contact lines (see Figs 13 and 14). Turning is most easily accomplished if the length of the ground contacts segments is small.

This method of turning not only affects the arch segment shape in the transition region, but also affects the whole sidewinder geometry. This turning process involves a 'twisting' of the arch segments as the robot moves through the transition, e.g. Fig. 15 shows a top view and a side view of the arch segment during the turning process. The touch-down point for each arch segment is slowly rotated so that the offset vector for each segment maintains the same length, but changes direction. This, like the

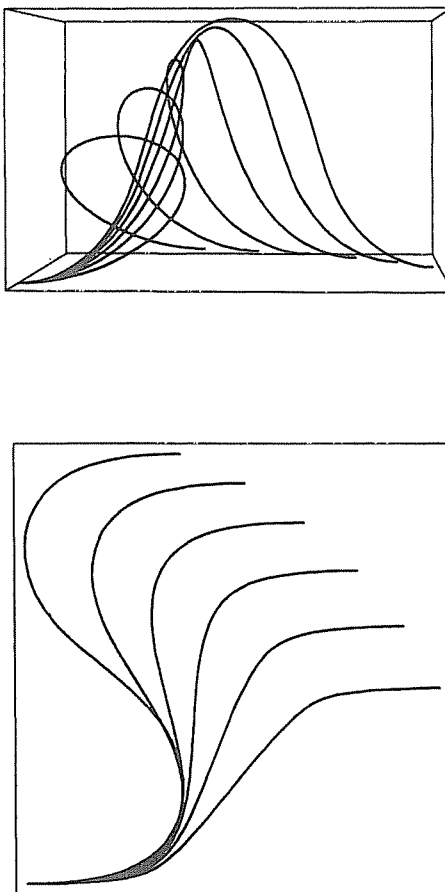


**Figure 15.** Side and top views of arch segment backbone curve during curvilinear turn sequence.

placement method of Section 5.1, involves using a less than optimal shape during the turning transition. But unlike the head placement method, a global change of direction can be accomplished because the direction of the parallel ground tracks has changed. This method can implement turns which are much sharper than the skew line method.

The major disadvantage of this turning method is computational cost. The arch segment shapes are time varying, and each segment shape is different. Thus, the modal Jacobian computational method must be repeatedly used on each arc segment. Further, at least three mode shapes are required for each arch segment.

## 6. CONCLUSION

This paper presented a novel analysis and a set of algorithms for hyper-redundant robot locomotion which is analogous to the sidewinding motion of desert snakes. The analysis in this paper focused on continuous morphology mechanisms, but we

showed by way of example that a discrete mechanical structure can also implement this gait.

This gait, which extends our previously developed repertoire of hyper-redundant locomotion gaits, is most useful for fast gross displacement. This paper did not consider sidewinding locomotion over uneven terrain. Sidewinding is really only feasible and advantageous over relatively level ground. We [2] developed algorithms for curvilinear locomotion over uneven terrain and used the same kinematic framework as in this paper, and thus it is possible to smoothly transition from a sidewinding gait to the curvilinear traveling or stationary wave gaits studied in [2].

### Acknowledgements

This work was supported by National Science Foundation grant MSS-901779, by NSF Presidential Young Investigator award MSS-9157843 and by the office of Naval Research Young Investigator Award N00014-92-J-1920.

### REFERENCES

1. G. S. Chirikjian and J. W. Burdick, "Kinematics of hyper-redundant locomotion with applications to grasping," in *Proc. IEEE Int. Conf. on Robotics and Automation*, Sacramento, CA, April 1991, pp. 720-725.
2. G. S. Chirikjian and J. W. Burdick, "The kinematics of hyper-redundant robotic locomotion," *IEEE Trans. Robotics Automat.*, in press.
3. J. Gray, *Animal Locomotion*. London: Weidenfeld and Nicolson, 1968.
4. G. S. Chirikjian and J. W. Burdick, "Design, implementation, and experiments with a 30 degree-of-freedom hyper-redundant robot," in *Proc. IEEE Int. Conf. on Robotics and Automation*, Atlanta, GA, May, 1993.
5. G. S. Chirikjian, "Theory and applications of hyper-redundant robotic manipulators," *PhD Thesis*, Department of Applied Mechanics, California Institute of Technology, 1992.
6. G. S. Chirikjian and J. W. Burdick, "A modal approach to hyper-redundant manipulator kinematics," *IEEE Trans. Robotics Automat.*, vol. 10, no. 3, pp. 343-354, 1994.
7. S. Hirose and Y. Umetani, "Kinematic control of active cord mechanism with tactile sensors," in *Proc. 2nd Int. CISM-IFT Symp. on Theory and Practice of Robots and Manipulators*, 1976, pp. 241-252.
8. S. Hirose, *Biologically Inspired Robots*. Oxford: Oxford University Press, 1993.
9. S. Hirose and A. Morishima, "Design and control of a mobile robot with an articulated body," *Int. J. Robotics Res.*, vol. 9, no. 2, pp. 99-114, 1990.
10. J. R. Stulce, W. E. Burgos, S. G. Dhande and C. F. Reinholz, "Conceptual design of a multibody passive-legged crawling vehicle," in *Proc. ASME Mechanisms Conf.*, Chicago, 1990.
11. T. Fukuda, H. Hosokai and M. Uemura, "Rubber gas actuator driven by hydrogen storage alloy for in-pipe inspection mobile robot with flexible structure," in *Proc. IEEE Int. Conf. on Robotics and Automation*, Scottsdale, AZ, May 1989, pp. 1847-1852.
12. B. C. Jayne, "Kinematics of terrestrial snake locomotion," *Copeia*, no. 4, pp. 915-927, 1986.
13. S. M. Secor, "Adaptive strategies of thermoregulation in free-ranging sidewinders *Crotalus-cerastes*," *Am. Zoolog.*, vol. 29, no. 4, p. 9, 1989.
14. B. M. Walton, B. C. Jayne and A. F. Bennet, "The cost of locomotion in the snake *Coluber constrictor*," *Am. Zoolog.*, vol. 29, no. 4, p. 22, 1989.
15. B. M. Walton, B. C. Jayne and A. F. Bennet, "The energetic cost of limbless locomotion," *Science*, vol. 249, pp. 524-527, 1990.
16. S. M. Secor, B. C. Jayne and A. F. Bennet, "Locomotor performance and energetic cost of sidewinding by the snake *Crotalus-cerastes*," *J. Exp. Biol.*, vol. 163, pp. 1-14, 1992.

17. N. Kopell and B. Ermentrout, "Coupled oscillators and the design of central Pattern generators," *Mathemat. Biosci.*, vol. 90, no. 1–2, pp. 87–109, 1988.
18. G. S. Chirikjian and J. W. Burdick, "Parallel formulation of the inverse kinematics of modular hyper-redundant manipulators," in *Proc. IEEE Int. Conf. on Robotics and Automation*, Sacramento, CA, April 1991, pp. 708–713.
19. M. P. DoCarmo, *Differential Geometry of Curves and Surfaces*. Englewood Cliffs, NJ: Prentice-Hall, 1976.
20. G. S. Chirikjian and J. W. Burdick, "Kinematically optimal hyper-redundant manipulator configurations," *IEEE Trans. Robotics Automat.*, in press.

## ABOUT THE AUTHORS

**Joel W. Burdick** received the BSME degree from Duke University in 1981, and the PhD degree in mechanical engineering from Stanford University in 1988. In May 1988 he started as an Assistant Professor in the Department of Mechanical Engineering at the California Institute of Technology, where he is now an Associate Professor. He is a National Science Foundation Presidential Young Investigator, an Office of Naval Research Young Investigator and the Hedges Feynman Fellow. His general research interests are in hyper-redundant robots, medical robots, dynamically stable legged locomotion and kinematic mobility theory.

**J. Radford** — information not available.



**Gregory S. Chirikjian** was born in August 1966 in New Brunswick, New Jersey, USA. He received the BSE degree in Engineering Mechanics and the MSE degree in Mechanical Engineering in 1988 while also fulfilling the requirements for a BA in Mathematics, all at The Johns Hopkins University. Between 1988 and 1992 he was a graduate student at the California Institute of Technology, where he received the PhD in Applied Mechanics in 1992. Since the summer of 1992 he has been an Assistant Professor in the Department of Mechanical Engineering at Johns Hopkins where he started the robotics program. His general research interests are in the analysis, design and implementation of 'hyper-redundant', 'metamorphic' and 'binary' manipulators. Dr Chirikjian is a National Science Foundation Young Investigator and a Presidential Faculty Fellow.